Available online at www.sciencedirect.com
SCIENCE DIRECT®
International Journal of Heat and Mass Transfer 49 (2006) 2397–2411
International Journal of HEAT and MASS TRANSFER
www.elsevier.com/locate/ijhmt

Exergetic analysis of fuel cell micropowerplants fed by methanol

Nico Hotz [a], Ming-Tsang Lee [a], Costas P. Grigoropoulos [a,*], Stephan M. Senn [b], Dimos Poulikakos [b]

[a] *University of California at Berkeley, Department of Mechanical Engineering, Laser Thermal Laboratory, 6177 Etcheverry Hall, Berkeley, CA 94720-1740, USA*
[b] *ETH Zurich, Department of Mechanical and Process Engineering, Laboratory of Thermodynamics in Emerging Technologies, ETH Zentrum, CH-8092 Zurich, Switzerland*

Received 17 July 2005; received in revised form 11 March 2006
Available online 24 April 2006

Abstract

In the present study, a hydrogen polymer electrolyte fuel cell (PEFC) micropowerplant in combination with a steam reformer fed by methanol and a direct methanol fuel cell (DMFC) micropowerplant are analyzed numerically regarding their exergetic efficiency. The effects of concentration and activation overpotentials, and ohmic resistance on the efficiency are considered in quasi-two-dimensional fuel cell models. The influence of significant operational parameters on the exergetic efficiency is examined numerically. Experimental results are conducted for the steam reformer. This work shows the importance of an exergy analysis of the fuel cell as part of an entire thermodynamic system generating electric power and compares PEFC and DMFC micropowerplants exergetically.

Keywords: Polymer electrolyte fuel cell; Direct methanol fuel cell; PEM fuel cell; Exergy analysis; Methanol; Efficiency

1. Introduction

Conventional power generation systems transform chemical energy of a fuel into useful electrical or mechanical power with an intermediate step of heat production. Heat is mainly generated by combustion, nuclear, or other reaction processes, which are responsible for significant energy loss. Fuel cells are a remarkable alternative for power generation transforming chemical energy directly into electric power and achieving higher efficiencies than conventional power generation systems. A promising application of fuel cells are fuel cell micropowerplants generating electric power at the order of some watts to power mobile devices such as cell phones, cameras, and notebooks. Fuel cell micropowerplants have the potential to replace rechargeable batteries used in mobile devices today.

A traditional method of analyzing power generation systems is an energetic analysis applying the first law of thermodynamics. However, it is clear that instead, an exergetic analysis with exergy as the measure of the quality of energy (useful part, transformable to work) can be used to specify design optima which are different than those resulting from the energy conservation law [1].

The objective of the present study is, first, the development of fuel cell models for a hydrogen polymer electrolyte fuel cell (PEFC) and a direct methanol fuel cell (DMFC), both using methanol as fuel. Existing one-dimensional (1-D) polarization models are extended for both fuel cell types to quasi-two-dimensional (quasi-2-D) fuel cell models. These extended fuel cell models are integrated into entire fuel cell systems, which are analyzed using the approach of exergetic efficiency. Specific requirements of an application such as fuel cell micropowerplants generating electric power of some watts are considered. Methanol is chosen as fuel because of its relatively easy and efficient storage in liquid phase. Since the systems have modular

* Corresponding author. Tel.: +1 510 642 2525; fax: +1 510 642 6163.
E-mail address: cgrigoro@me.berkeley.edu (C.P. Grigoropoulos).

0017-9310/$ - see front matter © 2006 Elsevier Ltd. All rights reserved.
doi:10.1016/j.ijheatmasstransfer.2006.03.007

Nomenclature

a	flow availability [W]
$\bar{a}$	molar availability [J mol^{-1}]
$\bar{a}^{\text{chem}}$	standard molar chemical availability [J mol^{-1}]
A	Arrhenius pre-factor [mol kg^{-1} s^{-1}]
A_{R}, B_{R}	Arrhenius pre-factors reforming reaction [m^3 kg^{-1} s^{-1}]
A_{dest}	exergy flow rate destruction [W]
b	width [m]
b^{a}, b^{c}	anode and cathode Tafel slope [V]
c	molar concentration [mol m^{-3}]
D	diffusion coefficient [m^2 s^{-1}]
E	cell voltage [V]
E^0	Nernst potential [V]
E_{R}, E_{D}	reforming, decomposition activation energy [J mol^{-1}]
F	Faraday constant (= 96,485 C mol^{-1})
$\bar{h}$	molar absolute enthalpy [J mol^{-1}]
i	current density [A m^{-2}]
k	reaction rate [mol m^{-3} s^{-1}]
k_{R}	reaction rate of reforming reaction [s^{-1}]
l	thickness [m]
L	length [m]
m	mass [kg]
M	molar mass [kg mol^{-1}]
n	molar flow rate [mol s^{-1}]
n^{d}	osmotic drag coefficient
n_{e}	number of electrons
n_{tubes}	number of reformer tubes
p	pressure [Pa]
P	power [W]
Q	heat transfer rate [W]
R	universal gas constant (= 8.3145 J mol^{-1} K^{-1})
R_{ohm}	ohmic resistance [Ω m^2]
$\bar{s}$	molar absolute entropy [J mol^{-1} K^{-1}]
S	surface area [m^2]
S_{c}	cross-sectional area [m^2]
T	absolute temperature [K]
u	velocity [m s^{-1}]
U	utilization factor
V	flow rate [m^3 s^{-1}]
w^m_{cat}	catalyst density [kg m^{-3}]
x	along-the-flow direction [m]
X	mole fraction
y	across-the-cell direction [m]
Y	mass fraction

Greek symbols

α	heat transfer coefficient [W m^{-2} K^{-1}]
α_{ct}	charge transfer coefficient
ε	effective porosity
η	conversion efficiency
η_{a}, η_{c}, η_{s}	anode, cathode, surface polarization [V]
φ	molar water/methanol ratio
Φ	phase potential [V]
κ, ψ	dimensionless parameter
λ	molar oxygen/fuel ratio
μ	exergetic efficiency
ρ	density [kg m^{-3}]
τ	tortuosity
ω	cross-over coefficient
Ω	overall effectiveness factor

Subscripts

b	backing layer
cat	catalyst
cl	catalyst layer
D, R, W	decomposition, reforming, water–gas shift reaction
h	channel
irr	irreversibility
s	surface
0	standard reference state (p = 1 atm, T_0 = 298 K)

Superscripts

a	anode
c	cathode

designs, different kinds of reformer as well as different fuels for the PEFC could be integrated in a straightforward manner. This study puts forward possibilities to increase the exergetic efficiency of a fuel cell micropowerplant by optimizing the operating conditions.

A major issue is to show the importance of analyzing the entire fuel cell systems in the sense of exergetic efficiency instead of dealing with the fuel cell as an isolated component. Considering the fuel cell micropowerplant as a small and mobile power generating device, aspects such as storage, pre-heating, vaporization, and reforming of the fuel as well as heat transfer between components for cooling and heating within a small space are essential. Analyzing only the fuel cell unit would mean neglecting these factors. The determining property of a mobile energy conversion device is the exergetic comparison between stored fuel and generated electric power. High exergetic efficiency means less fuel consumption, smaller storage tanks, lighter weight of the total system, and therefore lower operating costs leading to a marketable design. The exergetic analysis of fuel cell systems provides the possibility to compare the PEFC and the DMFC micropowerplants as different ways to use methanol as a fuel. The simple comparison of isolated PEFCs and DMFCs, as done in previous studies,

neglects exergetic losses in the entire system. In contrast to other studies performing an exergy analysis of fuel cell systems, this work uses complex fuel cell models considering voltage losses and mass transport in the cell. The combination of elaborate fuel cell models with an exergy analysis of the entire fuel cell micropowerplant, is another main objective of the present study.

2. Packed bed steam reforming of methanol

The highest performance of polymer electrolyte fuel cells can be achieved by using pure hydrogen as a fuel. However, the storage of hydrogen causes problems that have not been completely solved yet. Especially for fuel cell micropowerplants, a common solution is the on-board production of hydrogen by reforming or processing a hydrocarbon fuel. In this section, a packed bed steam reformer is presented as a possibility to use methanol as a fuel for an entire fuel cell micropowerplant.

2.1. Experimental setup

The fuel mixture consisting of methanol and water is stored in a liquid tank at room temperature. A pump transports the liquid water–methanol mixture to the vaporizer, where the liquid is evaporated at 350 K. A loose layer of silica wool inside the tube stabilizes the fluid flow and avoids sudden propulsion of liquid to the steam reformer. The water–methanol mixture flows in vaporized phase in the reformer glass tube including an isothermal packed bed of catalyst particles. The reformer temperature is in a range between 453 K and 523 K in this study. All needed geometric properties of the tube and the packed bed and the kinetic parameters of the catalyst are presented in Table 1.

Table 1
Parameters of the steam reformer

Parameters for the steam reformer experiments	Values
Inner glass tube	
Inner diameter (mm)	1.5
Packed bed	
Temperature T_{ref} (K)	453–523
Particle diameter (μm)	25.0
Mass of catalyst m_{cat} (mg)	15.0
Density of catalyst ρ_{cat} (kg m^{-3})	7671
Length of packed bed L (cm)	1.0
Kinetic parameters of catalyst	
Catalyst $Cu/ZnO/Al_2O_3$	
Pre-factor A_R (m^3 kg^{-1} s^{-1})	5.75×10^6
Pre-factor B_R (m^3 kg^{-1} s^{-1})	4.705×10^6
Activation energy E_R (kJ mol^{-1})	84.1
Pre-factor A_D (mol kg^{-1} s^{-1})	70.9×10^6
Activation energy E_D (kJ mol^{-1})	111.2
Fuel	
Molar water/methanol ratio φ_{ref}	1.1
Total liquid flow rate $V_{tot,in}$ (μL min^{-1})	2–20

2.2. Reacting flow model

The steam reforming of methanol is widely assumed to be composed of three global reactions: reforming, decomposition, and water–gas shift [2]. The reforming reaction reads

$$CH_3OH + H_2O \overset{k_R, k'_R}{\leftrightarrow} CO_2 + 3H_2, \tag{1}$$

and the decomposition reaction is given as

$$CH_3OH \overset{k_D}{\rightarrow} CO + 2H_2. \tag{2}$$

According to the simple reaction model of Amphlett et al. [2], the reforming reaction (1) is much faster than the decomposition reaction (2) and other reactions like the water–gas shift reaction. Therefore, only the reforming reaction and the decomposition reaction are considered in this study. Using the model for steam reforming of methanol by Park et al. [3], the reaction rate constant reads

$$k_R = (A_R + B_R \ln \varphi_{ref}) \exp[-E_R/(RT_{ref})] w'''_{cat} \tag{3}$$

for the reforming reaction and

$$k_D = A_D \exp[-E_D/(RT_{ref})] w'''_{cat} \tag{4}$$

for the decomposition reaction, respectively, where φ_{ref} is the molar ratio of water and methanol, R is the universal gas constant, T_{ref} is the reformer temperature, and w'''_{cat} is the catalyst density in the packed bed. The kinetic parameters A_i, B_R, and E_i of the used $Cu/ZnO/Al_2O_3$ catalyst are presented in Table 1.

Since the production of hydrogen by the decomposition reaction is much smaller than the production by the reforming reaction, these two reactions can be considered as decoupled [3]. By using the water–methanol ratio φ_{ref} and the conversion efficiency η_{ref}, the resulting reaction reads

$$CH_3OH + \varphi_{ref} H_2O \rightarrow 3\eta_{ref} H_2 + \eta_{ref} CO_2 + (1 - \eta_{ref}) CH_3OH + (\varphi_{ref} - \eta_{ref}) H_2O. \tag{5}$$

Note that the conversion efficiency η_{ref} is defined as the fraction of methanol converted to hydrogen. One-dimensional mass conservation of methanol relates the reaction kinetics to convective mass transport in the reformer tube, given by [3]

$$dn_{CH_3OH}/dx = -k_R c_{CH_3OH} S_c, \tag{6}$$

where n_{CH_3OH} is the molar flow rate of methanol, c_{CH_3OH} is the molar concentration of methanol in the differential reformer part, and S_c is the cross-sectional area of the reformer tube. According to Park et al. [3], the mass conservation equation of methanol (see Eq. (6)) can be rewritten as

$$\frac{u_{in}}{1 + \varphi_{ref}} \frac{d\eta_{ref}}{dx} = k_R \frac{1 - \eta_{ref}}{1 + \varphi_{ref} + 2\eta_{ref}}, \tag{7}$$

where u_{in} is the superficial flow velocity at the inlet of the reformer. Integration of Eq. (7) results in an implicit

expression for the conversion efficiency η_{ref} in dependence of the axial coordinate x, given by

$$x = -\frac{u_{in}}{k_R}\left[\frac{3+\varphi_{ref}}{1+\varphi_{ref}}\ln(1-\eta_{ref}) + \frac{2}{1+\varphi_{ref}}\eta_{ref}\right]. \quad (8)$$

In addition, the mole fraction of carbon monoxide (CO) X_{CO} in the reformed gas mixture has to be determined. This value is crucial for the fuel cell, since CO poisons the fuel cell catalysts. The molar flow rate of CO changes along the flow direction according to the decomposition reaction (2)

$$dn_{CO}/dx = k_D S_c, \quad (9)$$

where n_{CO} is the molar flow rate of CO. According to Park et al. [3], the influence of the decomposition reaction on the total molar flow rate n_{tot} can be neglected, because the reforming reaction (1) is much faster than the decomposition reaction (2). The total molar flow rate n_{tot} is therefore assumed to be only affected by reaction (1). With stoichiometry from (5), Eq. (9) reads

$$\frac{d}{dx}[X_{CO}(1+\varphi_{ref}+2\eta_{ref})] = \frac{k_D S_c}{n_{CH_3OH,in}}, \quad (10)$$

which leads to the distribution of the CO mole fraction X_{CO} along the flow direction, given by

$$X_{CO} = \frac{k_D S_c}{n_{CH_3OH,in}}\frac{x}{1+\varphi_{ref}+2\eta_{ref}}. \quad (11)$$

Note that the conversion efficiency η_{ref} depends on the axial coordinate x (see Eq. (8)).

3. Model of a hydrogen PEFC

A simple 1-D model developed by Gurau et al. [4] is used in this study. The performance of the PEFC using hydrogen as a fuel is assumed to be mainly determined by reaction and diffusion processes on the cathode side of the fuel cell. The entire fuel cell can be described by a 1-D half-cell model of the cathode side consisting of a cathode gas channel, a gas diffusion layer, a catalyst layer, and a fuel cell membrane, as presented in [4]. The diffusion of oxygen across the half-cell is calculated by the Fick's law [4], considering the effective porosity ε and the tortuosity τ of the gas diffusion layer and the catalyst layer, and the consumption of oxygen by the fuel cell reaction in the catalyst layer. The cell voltage E

$$E = E^0 - \Delta\Phi - \eta_s \quad (12)$$

is given as a function of the cathode surface overpotential η_s, the membrane phase potential between anode and cathode $\Delta\Phi$, and the ideal reversible voltage or Nernst potential E^0. The current density of the fuel cell i, written as a function of the surface overpotential η_s, reads

$$i = n_e F k \exp[\eta_s \alpha_{ct} n_e F/(RT)] l_{cl} \Omega Y_{O_2}, \quad (13)$$

where k is the reaction rate constant of the fuel cell reaction and l_{cl} is the thickness of the catalyst layer. The overall effectiveness factor Ω is given in [4]. The polarization curve can be described parametrically by Eqs. (12) and (13), using the surface overpotential η_s as an independent variable. All necessary parameters from Gurau et al. [4] are given in Table 2.

A major issue for any PEFC using hydrocarbon or alcohol reformate feed is the inevitable CO concentration in the anode gas. CO occupies catalytically active sites on the anode and therefore, CO impedes the reaction of hydrogen on the anode and leads to reduced current densities. This CO poisoning of the anode is investigated in several recent studies, e.g. [5,6], and numerical models are developed to consider the anode CO kinetics, especially for CO mole fractions in the range of 10 and 100 ppm. However, these studies [5,6] show that the effect of CO poisoning is marginal for CO mole fractions below 10 ppm. Since the purpose of this study is the exergetic comparison of two methanol micropowerplants and not the development of an extensive PEFC model, the approximation of a PEFC half-cell model is used. This assumption is valid if the CO mole fraction on the anode side of the PEFC is clearly below 10 ppm. This requirement is fulfilled for the results presented in this study.

In this study, the 1-D model developed by Gurau et al. [4] is extended to a quasi-2-D isothermal PEFC model. The 1-D model is used to describe the diffusion and reaction processes across the fuel cell. To consider the profiles of species concentrations along the anode and cathode channels, the channels are discretized. The variations of species concentrations lead to a non-uniform current density distribution along the fuel cell. Pressure losses in the channels are neglected. The cell voltage E is fixed as an operational parameter. Using Eqs. (12) and (13), the resulting surface overpotential η_s and the current density i can be calculated. The molar flow rates of hydrogen, water, and oxygen change along the fuel cell channels. The gradients in molar flow rate of hydrogen in the anode channel and oxygen in the cathode channel read

$$dn^a_{H_2}/dx = 2dn^c_{O_2}/dx = -bi/(2F), \quad (14)$$

the gradient of molar water flow rate in the anode channel reads

$$dn^a_{H_2O}/dx = -bn^d_{H_2O} i/F, \quad (15)$$

and the gradient of molar water flow rate in the cathode channel is given by

$$dn^c_{H_2O}/dx = b(1/2 + n^d_{H_2O})i/F, \quad (16)$$

where $n^d_{H_2O}$ is the osmotic drag coefficient given by [7] and b is the cell width. The gradient of generated electric power dP along the flow direction x for constant cell voltage E is written as

$$dP/dx = biE, \quad (17)$$

where the current density i is calculated using Eq. (13). The energy conservation equation reads

Table 2
Parameters of the PEFC and DMFC model

Parameters of the PEFC model by Gurau et al. [4]	Values
Fuel cell temperature T_{pefc} (K)	353
Reaction rate constant k (mol m^{-3} s^{-1})	0.015
Charge transfer coefficient α_{ct}	1.0
Thickness of the gas channel l_{h} (mm)	1.0
Thickness of the gas diffusion layer l_{gdl} (μm)	350
Thickness of the catalyst layer l_{cl} (μm)	10
Thickness of the membrane l_m (μm)	50
Effective porosity of the gas diffusion layer $\varepsilon_{\mathrm{gdl}}$	0.7
Tortuosity of the gas diffusion layer τ_{gdl}	1.5
Effective porosity of the catalyst layer $\varepsilon_{\mathrm{cl}}$	0.2
Tortuosity of the catalyst layer τ_{cl}	1.5
Volume fraction of ionomer in catalyst layer ε	0.136
Ionomer tortuosity in catalyst layer τ	1.5
Nernst potential E^0 (V)	1.23
Molar chemical availability by Moran and Shapiro [10]	
Molar chemical availability H_2 $\bar{a}^{\mathrm{chem}}_{H_2}$ (kJ mol^{-1})	236.1
Molar chemical availability O_2 $\bar{a}^{\mathrm{chem}}_{O_2}$ (kJ mol^{-1})	3.97
Molar chemical availability N_2 $\bar{a}^{\mathrm{chem}}_{N_2}$ (kJ mol^{-1})	0.72
Molar chemical availability CO_2 $\bar{a}^{\mathrm{chem}}_{CO_2}$ (kJ mol^{-1})	19.87
Molar chemical availability CH_4 $\bar{a}^{\mathrm{chem}}_{CH_4}$ (kJ mol^{-1})	831.65
Molar chemical availability CO $\bar{a}^{\mathrm{chem}}_{CO}$ (kJ mol^{-1})	275.1
Molar chemical availability gaseous H_2O $\bar{a}^{\mathrm{chem}}_{H_2O}$ (kJ mol^{-1})	9.5
Molar chemical availability liquid H_2O $\bar{a}^{\mathrm{chem}}_{H_2O,l}$ (kJ mol^{-1})	0.9
Molar chemical availability gaseous CH_3OH $\bar{a}^{\mathrm{chem}}_{CH_3OH}$ (kJ mol^{-1})	722.3
Molar chemical availability liquid CH_3OH $\bar{a}^{\mathrm{chem}}_{CH_3OH,l}$ (kJ mol^{-1})	718.0

Parameters of the DMFC model by Kulikovsky [12]	$T = 343$ K	$T = 353$ K	$T = 363$ K
Tafel slope of anode b^{a} (V)	0.0369	0.0419	0.0450
Tafel slope of cathode b^{c} (V)	0.0468	0.0443	0.0430
Characteristic anode current density $i^{\mathrm{a}}_{\mathrm{ch}}$ (A cm^{-2})	2.74	3.70	4.67
Characteristic cathode current density $i^{\mathrm{c}}_{\mathrm{ch}}$ (A cm^{-2})	1.86	2.78	2.62
Dimensionless parameter ψ	5.25	3.72	6.46
Dimensionless parameter $\ln\kappa = \ln\kappa^{\mathrm{a}}_{\mathrm{h}} b^{\mathrm{a}}/b^{\mathrm{c}} + \ln\kappa^{\mathrm{c}}_{\mathrm{h}}$	21.0	21.0	21.0
Diffusion coefficient of liquid methanol $D^{\mathrm{a}}_{\mathrm{CH_3OH,b}}$ (m^2 s^{-1})	6.7×10^{-10}	7.8×10^{-10}	14.0×10^{-10}
Diffusion coefficient of oxygen $D^{\mathrm{c}}_{\mathrm{O_2,b}}$ (m^2 s^{-1}) [13]	4.4×10^{-6}	4.7×10^{-6}	4.9×10^{-6}
Thickness of the anode backing layer $l^{\mathrm{a}}_{\mathrm{b}}$ (mm)	0.2	0.2	0.2
Thickness of the cathode backing layer $l^{\mathrm{c}}_{\mathrm{b}}$ (mm)	0.2	0.2	0.2
Ohmic resistance R_{ohm} (Ω cm^2)	0.202	0.243	0.256
Nernst potential E^0 (V) [14]	1.21	1.21	1.21

$$\mathrm{d}Q_{\mathrm{pefc}}/\mathrm{d}x = -\mathrm{d}P/\mathrm{d}x - \mathrm{d}h^{\mathrm{a}}_{\mathrm{h}}/\mathrm{d}x - \mathrm{d}h^{\mathrm{c}}_{\mathrm{h}}/\mathrm{d}x, \tag{18}$$

where the absolute enthalpies of the flows in the anode and cathode channel, $h^{\mathrm{c}}_{\mathrm{h}}$ and $h^{\mathrm{a}}_{\mathrm{h}}$, are given by

$$h_{\mathrm{h}} = \sum_j n_j \bar{h}_{\mathrm{h,j}}. \tag{19}$$

The index j refers to the species in the channels. The molar absolute enthalpies $\bar{h}$ as well as the molar absolute entropies $\bar{s}$ include the enthalpy and entropy of formation, respectively, and are determined from the polynomial equations [8]

$$\bar{h} = RT(\beta_1 + T\beta_2/2 + T^2\beta_3/3 + T^3\beta_4/4 + T^4\beta_5/5 + \beta_6/T) \tag{20}$$

and

$$\bar{s} = R(\ln(T)\beta_1 + T\beta_2 + T^2\beta_3/2 + T^3\beta_4/3 + T^4\beta_5/4 + \beta_7), \tag{21}$$

where the coefficients β_j can be found in JANAF tables [9]. The fuel cell is operated isothermally at a temperature T_{pefc}. In addition, the exergy destruction $\mathrm{d}A_{\mathrm{dest,pefc}}$ along the flow direction varies with

$$\mathrm{d}A_{\mathrm{dest,pefc}}/\mathrm{d}x = -(1 - T_0/T_{\mathrm{pefc}})\mathrm{d}Q_{\mathrm{pefc}}/\mathrm{d}x - \mathrm{d}P/\mathrm{d}x - \mathrm{d}a^{\mathrm{a}}_{\mathrm{h}}/\mathrm{d}x - \mathrm{d}a^{\mathrm{c}}_{\mathrm{h}}/\mathrm{d}x, \tag{22}$$

where the availability of the species flows in the anode and cathode channel, $a^{\mathrm{a}}_{\mathrm{h}}$ and $a^{\mathrm{c}}_{\mathrm{h}}$, are given by

$$a_{\mathrm{h}} = \sum_j n_j \bar{a}_{\mathrm{h,j}}. \tag{23}$$

The molar flow availability $\bar{a}_j$ is defined as

$$\bar{a}_j = (\bar{h}_j(T) - \bar{h}_j(T_0)) - T_0(\bar{s}_j(T) - \bar{s}_j(T_0)) + RT_0 \ln(X_j) + \bar{a}_j^{\text{chem}}. \quad (24)$$

The index j refers to the species in the channels. The molar absolute enthalpy $\bar{h}$ and the molar absolute entropy $\bar{s}$ are defined by Eqs. (20) and (21), respectively. The molar chemical availabilities $\bar{a}_j^{\text{chem}}$ are given in Table 2, according to the reference environment model II of Table A-26 of [10]. The total electric power generated by the fuel cell and the total heat released from the fuel cell to the environment are obtained by integration of Eqs. (17) and (18) over the cell length L. An important performance parameter of the fuel cell is the utilization factor of hydrogen

$$U_{H_2} = (n^a_{H_2,in} - n^a_{H_2,out})/n^a_{H_2,in}, \quad (25)$$

indicating the fraction of hydrogen that is converted in the fuel cell. The parameter

$$\lambda_{pefc} = n^c_{O_2,in}/(n^a_{H_2,in}/2) \quad (26)$$

is the molar ratio of oxygen and stoichiometric oxygen at the fuel cell inlets.

4. PEFC micropowerplant

A thermodynamic model of a PEFC micropowerplant, including a reformer performing steam reformation of methanol, a post-combustor with heat exchangers, a vaporizer, a preferential oxidation (PROX) reactor to remove CO, and a pre-heater, arranged according to Fig. 1(a), is introduced in this section. The components of the system are modeled as control volumes, except for the fuel cell and the steam reformer, which are modeled according to the previous Sections 2 and 3. For every component of the system, a mass balance, an energy balance, and an exergy balance can be formulated. Conservation of mass at steady state for a certain system component requires that the inlet flow rates of hydrogen, carbon, oxygen, and nitrogen have to be the same as the outlet flow rates, i.e.

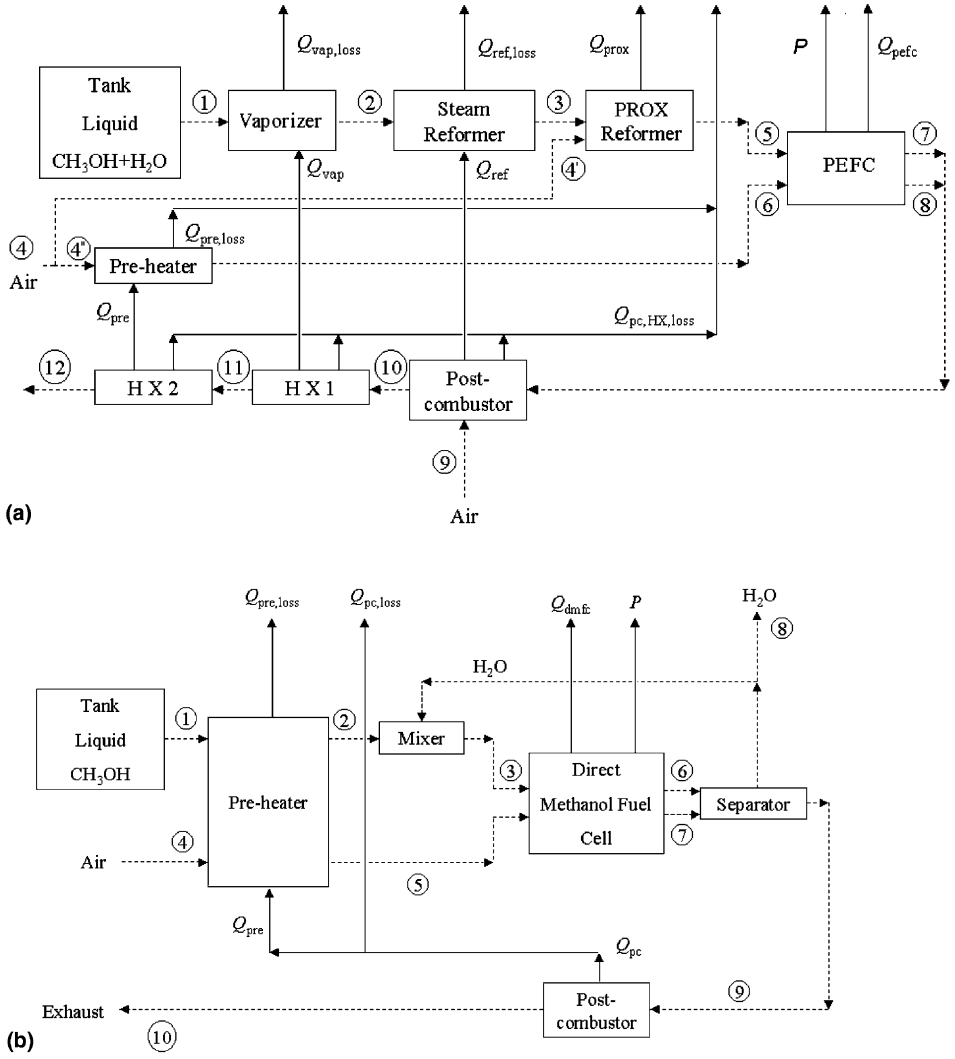

Fig. 1. (a) Schematic of the PEFC micropowerplant and (b) the DMFC micropowerplant.

$$\sum_j n_{\mathrm{in,j}} = \sum_j n_{\mathrm{out,j}}, \tag{27}$$

where j refers to the elements H, C, O, and N. Other elements are neglected in this study, since only the input of methanol, water, and air is considered, where the inlet air is assumed to consist of 21% oxygen and 79% nitrogen. The entire fuel cell system is assumed to be isobaric at atmospheric state. Pressure losses in the system and the required pumping power due to the pressure drop in the packed bed steam reformer are neglected. The change of kinetic and potential energy is neglected. The energy balance of a certain system component then reads

$$\sum_j n_{\mathrm{in,j}} \bar{h}_{\mathrm{in,j}} + Q_{\mathrm{in}} = \sum_j n_{\mathrm{out,j}} \bar{h}_{\mathrm{out,j}} + Q_{\mathrm{out}} + P, \tag{28}$$

where n is the molar flow rate, Q is the heat transfer rate, P is the generated power, and $\bar{h}$ is the molar absolute enthalpy, including the enthalpy of formation and calculated by the JANAF tables [8] according to Eq. (20). Note that the subscripts "in" and "out" refer to the inlets and outlets of the system component, respectively. An exergy balance is formulated to calculate the exergy destruction A_{dest} across a system component

$$A_{\mathrm{dest}} = (1 - T_0/T_{\mathrm{s}})Q_{\mathrm{in}} - (1 - T_0/T_{\mathrm{s}})Q_{\mathrm{out}} - P + a_{\mathrm{in}} - a_{\mathrm{out}}, \tag{29}$$

using the definition of flow availability a of Eq. (23). Note that T_{s} is the mean temperature of the surface at the boundary of the component subject to the heat transfer Q and T_0 is the ambient temperature. For the vaporizer, the pre-heater, the post-combustor, and its heat exchangers, a mean temperature is defined as

$$T_{\mathrm{s}} = (T_{\mathrm{in}} + T_{\mathrm{out}})/2, \tag{30}$$

whereas the steam reformer and the PEFC are assumed to be isothermal with

$$T_{\mathrm{s}} = T_{\mathrm{in}} = T_{\mathrm{out}}. \tag{31}$$

Using the mean temperatures of the vaporizer, the steam reformer, the pre-heater, the post-combustor, and its heat exchangers, the heat loss to the environment Q_{loss} by each component is calculated by

$$Q_{\mathrm{loss}} = \alpha S(T_{\mathrm{s}} - T_0), \tag{32}$$

with an effective average heat transfer coefficient α and the participating component surface area S.

The vaporizer evaporates the stored liquid water–methanol mixture and pre-heats the generated vapor. The reformer converts methanol and water by steam reforming to hydrogen, carbon dioxide (CO_2), and CO. The mathematical model of the steam reformer is described in Section 2. The reformer is built as a bundle of n_{tubes} tubes, each tube like the packed bed tube presented in Section 2. The efficiency of conversion η_{ref} can be calculated by Eq. (8) and therefore, the molar flow rates of CH_3OH, H_2O, H_2, CO_2, and CO at the outlet state 3 are defined. The mole fraction of CO in the product gas of the steam reformer is typically in the order of a few 100 ppm. However, mole fractions of CO above 100 ppm poison the catalysts of the PEFC immediately. To avoid poisoning during long-term periods of operation, the critical CO mole fraction has to be even below 10 ppm, as shown by [5,6]. The necessary CO removal can be achieved by oxidation of CO by a PROX reformer, e.g. using a platinum catalyst to oxidize CO without depleting hydrogen. By mixing a small amount of air to the gas mixture of the steam reformer consisting of H_2, CO_2, CH_3OH, H_2O, and CO, two main reactions take place. First,

$$2\mathrm{CO} + \mathrm{O_2} \rightarrow 2\mathrm{CO_2} \tag{33}$$

is the desired removal of CO, whereas

$$2\mathrm{H_2} + \mathrm{O_2} \rightarrow 2\mathrm{H_2O} \tag{34}$$

removes usable hydrogen. Other reactions are neglected. Previous studies like [11] have achieved CO conversion of 99% and therefore small losses of hydrogen for inlet CO mole fractions of 1000 ppm and a reaction temperature $T_{\mathrm{prox}} = 443$ K. For the results of this study, the CO mole fraction at the outlet of the steam reformer is in the range of 50 to almost 1000 ppm. For results where CO poisoning is negligible and the achieved exergetic efficiency of the system is satisfactory, the CO mole fraction after the PROX reformer is between 1 and 4 ppm. The conversion efficiency of the PROX reformer η_{prox} is defined as

$$\eta_{\mathrm{prox}} = (n_{\mathrm{CO,3}} - n_{\mathrm{CO,5}})/n_{\mathrm{CO,3}}. \tag{35}$$

According to [11], the optimal ratio of air and stoichiometric air

$$\lambda_{\mathrm{prox}} = n_{\mathrm{O_2,4'}}/(n_{\mathrm{CO,3}}/2) \tag{36}$$

for these conditions is around 4.0. Reaction (34) reduces the amount of hydrogen to

$$n_{\mathrm{H_2,5}} = n_{\mathrm{H_2,3}} - (4 - \eta_{\mathrm{prox}})n_{\mathrm{CO,3}}. \tag{37}$$

Since $n_{\mathrm{CO,3}} \ll n_{\mathrm{H_2,3}}$, the loss of hydrogen is small. The molar flow rate of methanol is constant within the PROX reformer. Since the PROX reaction is exothermal, heat has to be released to the environment to keep the PROX reformer isothermal at an optimal PROX temperature T_{prox}. Further, it is assumed that the inlet gas mixture is cooled from $T_3 = T_{\mathrm{ref}}$ to T_{prox} and then to the lower fuel cell temperature $T_5 = T_{\mathrm{pefc}}$. The necessary heat transfer rate Q_{prox} between PROX and the ambient environment is calculated by Eq. (28), and the exergy destruction by Eq. (29).

The airflow to the hydrogen PEFC is pre-heated for isothermal conditions in the fuel cell. An essential parameter of this study is the exergetic efficiency μ of the entire PEFC micropowerplant, defined as the ratio between the exergy output (i.e., the generated electric power P) and the exergy input (i.e., the flow availability of methanol and water at state 1 and air at the states 4 and 9), given as

$$\mu = P/(a_1 + a_4 + a_9), \tag{38}$$

where the flow availabilities a are defined by Eq. (23).

A major issue in PEFCs is the water management, since a certain hydration of the membrane has to be guaranteed for every operational point to ensure satisfactory performance. In this study, the problem of hydration is less crucial than in many other studies, because the feeding gas mixture on the anode side contains a significant amount of water vapor from the steam reformer.

In the post-combustor, remaining CH_3OH, H_2, and CO from the fuel cell exhaust are burnt to provide heat for preheating and to avoid exhaust of CO and unburnt hydrocarbons. The post-combustor consists of three different parts to consider three different steps of heat transfer taking place at different temperature levels. In the first stage, the remaining fuel is burnt and heat is transferred to the steam reformer, which requires heat input at the highest temperature. The first heat exchanger (HX1) heats the vaporizer, the second heat exchanger (HX2) releases heat to the air pre-heater at the lowest temperature level. In the heat exchangers, no reactions take place. The heat transport within the system is shown in Fig. 1(a). The heat released from the fuel cell Q_{pefc} and the PROX reformer Q_{prox} is rejected to the environment, whereas the heat released from the post-combustor is used to heat the vaporizer (Q_{vap}), the steam reformer (Q_{ref}), and the pre-heater (Q_{pre}). All components reject heat to the environment because of imperfect insulation. The total heat released to the environment Q_{rel} reads

$$Q_{\mathrm{rel}} = Q_{\mathrm{vap,loss}} + Q_{\mathrm{ref,loss}} + Q_{\mathrm{pre,loss}} + Q_{\mathrm{prox}} + Q_{\mathrm{pefc}} + Q_{\mathrm{pc,HX,loss}}. \quad (39)$$

The results will show that the post-combustor can easily provide the needed amount of heat.

The total exergy destruction by irreversibilities in system components is given as

$$A_{\mathrm{dest,irr}} = A_{\mathrm{dest,vap}} + A_{\mathrm{dest,ref}} + A_{\mathrm{dest,prox}} + A_{\mathrm{dest,pre}} + A_{\mathrm{dest,pefc}} + A_{\mathrm{dest,pc,HX}}, \quad (40)$$

and the exergy destruction by heat transfer $A_{\mathrm{dest,heat}}$ is given as

$$A_{\mathrm{dest,heat}} = a_1 + a_4 + a_9 - a_{12} - A_{\mathrm{dest,irr}} - P. \quad (41)$$

5. DMFC model

In a DMFC, liquid methanol is directly used as a fuel without conversion to hydrogen. On the anode side, methanol and water react to produce CO_2 and hydrogen ions. The anode reaction reads

$$CH_3OH + H_2O \rightarrow CO_2 + 6H^+ + 6e^-, \quad (42)$$

and the cathode reaction reads

$$3/2O_2 + 6H^+ + 6e^- \rightarrow 3H_2O. \quad (43)$$

A 1-D DMFC model developed by Kulikovsky [12] is used in this study to determine the voltage losses due to activation barriers, diffusion resistances for the reacting species and products, and ohmic losses. The polarization voltage caused by diffusion and activation resistances in a DMFC depends on the current density i, the molar concentration of methanol in the anode channel $c^{\mathrm{a}}_{\mathrm{CH_3OH,h}}$, and the molar concentration of oxygen in the cathode channel $c^{\mathrm{c}}_{\mathrm{O_2,h}}$ [12]. The polarization voltage of the anode and cathode side read η_{a} and η_{c}, respectively. The cell voltage E of the DMFC is the difference between the ideal reversible potential or Nernst potential E^0 and the sum of all polarization voltages, written as

$$E = E^0 - \eta_{\mathrm{a}} - \eta_{\mathrm{c}} - R_{\mathrm{ohm}} i, \quad (44)$$

where R_{ohm} considers ohmic losses in the membrane and the contacts. All parameters needed to match the results with experimental data are taken from [12] and are presented in Table 2.

Using Eq. (44), the current density i can be calculated with the cell voltage E fixed as an operational parameter. In a quasi-2-D DMFC model, the molar flow rates of CH_3OH, CO_2, H_2O, and O_2 change along the fuel cell channels. The methanol transported to the cathode side by cross-over is assumed to react immediately with O_2 to CO_2 and H_2O [12]. The changes in molar flow rate of methanol in the anode channel and oxygen in the cathode channel read

$$\mathrm{d}n^{\mathrm{a}}_{\mathrm{CH_3OH}}/\mathrm{d}x = (2/3)\mathrm{d}n^{\mathrm{c}}_{\mathrm{O_2}}/\mathrm{d}x = -(1 + 6n^{\mathrm{d}}_{\mathrm{CH_3OH}})bi/(6F), \quad (45)$$

the change in molar flow rate of CO_2 in the anode channel reads

$$\mathrm{d}n^{\mathrm{a}}_{\mathrm{CO_2}}/\mathrm{d}x = bi/(6F), \quad (46)$$

the change in molar flow rate of H_2O in the anode channel is given by

$$\mathrm{d}n^{\mathrm{a}}_{\mathrm{H_2O}}/\mathrm{d}x = -(1 + 6n^{\mathrm{d}}_{\mathrm{H_2O}})bi/(6F), \quad (47)$$

the change in molar flow rate of CO_2 in the cathode channel is given by

$$\mathrm{d}n^{\mathrm{c}}_{\mathrm{CO_2}}/\mathrm{d}x = n^{\mathrm{d}}_{\mathrm{CH_3OH}}bi/F, \quad (48)$$

and the change in molar flow rate of H_2O in the cathode channel reads

$$\mathrm{d}n^{\mathrm{c}}_{\mathrm{H_2O}}/\mathrm{d}x = (1 + 2n^{\mathrm{d}}_{\mathrm{H_2O}} + 4n^{\mathrm{d}}_{\mathrm{CH_3OH}})bi/(2F), \quad (49)$$

where the osmotic drag coefficients n^{d}_j are given by [7] and b is the fuel cell width. It is assumed that the ratio of dragged water molecules to dragged methanol molecules depends on the ratio of their concentrations. The variation of the generated electric power P along the flow direction x is written as

$$\mathrm{d}P/\mathrm{d}x = biE, \quad (50)$$

where the current density i is given by Eq. (44). The isothermal energy conservation reads

$$dQ_{dmfc}/dx = -dP/dx - dh_h^a/dx - dh_h^c/dx, \quad (51)$$

where the absolute flow enthalpies in the anode and cathode channel, h_h^a and h_h^c, are calculated by Eq. (19). In addition, the exergy destruction $dA_{dest,dmfc}$ is computed by

$$dA_{dest,dmfc}/dx = -(1 - T_0/T_{dmfc})dQ_{dmfc}/dx - dP/dx - da_h^a/dx - da_h^c/dx, \quad (52)$$

where the flow availabilities a are given in Eq. (23). The total electric power generated by the fuel cell and the heat released from the DMFC to the environment are given by the integrals of Eqs. (50) and (51). An important performance parameter of the fuel cell is the utilization factor of methanol

$$U_{CH_3OH} = (n^a_{CH_3OH,in} - n^a_{CH_3OH,out} - n^c_{CH_3OH,out})/n^a_{CH_3OH,in}, \quad (53)$$

indicating the amount of methanol that is converted in the fuel cell. The parameter

$$\lambda_{dmfc} = n^c_{O_2,in}/(1.5 n^a_{CH_3OH,in}) \quad (54)$$

is the molar ratio between oxygen and stoichiometric oxygen at the fuel cell inlet. The cross-over coefficient for methanol ω_{CH_3OH}, defined as the molar ratio of methanol at the cathode outlet and methanol at the anode inlet, is given by

$$\omega_{CH_3OH} = n^c_{CH_3OH,out}/n^a_{CH_3OH,in}. \quad (55)$$

The molar ratio between water and methanol φ_{dmfc} at the anode inlet is defined as

$$\varphi_{dmfc} = n^a_{H_2O,in}/n^a_{CH_3OH,in}. \quad (56)$$

6. DMFC micropowerplant

A schematic of a DMFC micropowerplant is shown in Fig. 1(b). The presented micropowerplant consists of three main components: a pre-heater to heat methanol and air to the fuel cell temperature, the fuel cell itself, and a post-combustor to provide heat for the pre-heating and to burn remaining methanol in the exhaust gas. The methanol is stored in liquid phase at ambient conditions and it is mixed in a small mixing device with liquid water being separated from gaseous fuel cell products in a separator. Both the DMFC and the post-combustor release heat. It is assumed that the entire heat from the fuel cell is lost to the environment. Heat from the post-combustor is used in the pre-heater, and excess heat is rejected to the environment. The pre-heating of methanol and air to a fuel cell temperature below 365 K needs clearly less heat than the fuel cell itself rejects. The DMFC can never use the entire amount of methanol, which always leads to a certain amount of fuel in the post-combustor to provide heat by combustion.

The DMFC, the mixer, and the separator are assumed to be isothermal at T_{dmfc}. For the pre-heater and the post-combustor, a mean temperature T_s is defined by Eq. (30). The heat $Q_{pre,loss}$ released to the environment as a consequence of the temperature difference between pre-heater and the ambient temperature is calculated by Eq. (32). The mass, energy, and exergy conservation equations are given for all components by Eqs. (27)–(29).

Since water is the only liquid species in the otherwise gaseous fuel cell product, the separation of liquid water in the separator is assumed to take place without any power input. Both separator and mixer are assumed to be isothermal and adiabatic. Most of the water is recycled in the mixer, only excess water is rejected to the environment at state 8. The exergy destruction by the separator is not calculated explicitly. In this study, for the air/fuel ratio always $\lambda_{dmfc} \geqslant 1$ applies, since variation of the air/fuel ratio has no significant effect on the performance of the DMFC. For this reason, there is always enough oxygen in the post-combustor to ensure complete combustion of the methanol.

An essential parameter of this study is the exergetic efficiency μ of the entire DMFC micropowerplant, defined as the ratio between the exergy output (i.e., the electric power P) and the exergy input (i.e., the flow availability of methanol at state 1 and air at state 4), given as

$$\mu = P/(a_1 + a_4), \quad (57)$$

with the flow availabilities a defined in Eq. (23). The irreversible exergy destruction $A_{dest,irr}$ reads

$$A_{dest,irr} = A_{dest,pre} + A_{dest,mix} + A_{dest,dmfc} + A_{dest,pc} \quad (58)$$

and the exergy destruction by heat transfer and by the separator ($A_{dest,heat} + A_{dest,sep}$) is calculated by

$$A_{dest,heat} + A_{dest,sep} = a_1 + a_4 - a_8 - a_{10} - A_{dest,irr} - P. \quad (59)$$

7. Numerical solution

For both fuel cell systems, the numerical integration along the flow direction in the fuel cells is accomplished using a fourth-order Runge–Kutta method. For the calculations presented in this study, the results converge fast. For a discretization with 10 (50, 100, 200) spatial increments, the relative error of the resulting exergetic efficiency of the PEFC micropowerplant is 5.2% (0.6%, 0.2%, 0.1%). In the case of the DMFC micropowerplant, the situation is similar: For 10 (50, 100, 200) spatial increments, the relative error of the exergetic efficiency is 3.4% (0.6%, 0.3%, 0.2%). In this study, a discretization with 200 spatial increments is used for the PEFC and the DMFC system. The mass, energy, and exergy conservation within each system component and within the entire system are checked for all calculation.

8. Results

8.1. Packed bed steam reformer

In Fig. 2, the numerical calculations of the reforming efficiency are compared with experimental results. For the

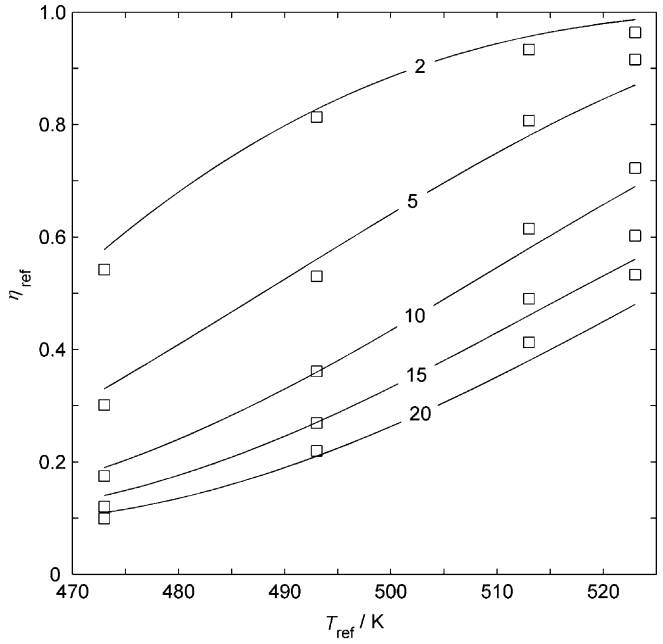

Fig. 2. The calculated conversion efficiency of the steam reformer η_{ref} as a function of the reformer temperature T_{ref} for different inlet flow rates $V_{tot,in}$, indicated in μL min^{-1}. The squares represent the new experimental results achieved for this study with an improved catalyst from BASF.

experiments of this study, an improved catalyst from BASF is used. The catalytic properties calculated from experimental data of this study using the reacting flow model are listed in Table 1. The squares in Fig. 2 represent the experimental results, achieved for different inlet flow rates of water–methanol mixture $V_{tot,in}$ and temperatures T_{ref} between 470 K and 525 K. The water/methanol molar ratio $\varphi_{ref} = 1.1$. The experimental setup is described in Section 2.1. The discrepancy between numerical and experimental results is explained by imperfect experimental conditions such as non-uniform temperature distribution in the reformer tube and by the simplifying reacting flow model that considers only two decoupled reactions, whereas the real reaction mechanism is much more complex. However, the agreement of experimental and numerical results is satisfactory, especially for lower temperatures. To decrease the mole fraction of CO in the outlet flow, the reformer temperature should be relatively low, which decreases the conversion efficiency η_{ref}. Fig. 2 shows that the conversion efficiency can be kept on a relatively high level for low temperatures, if the inlet flow rates are small.

8.2. PEFC micropowerplant

The electric power and exergetic efficiency of the PEFC micropowerplant is calculated for a standard case defined in Table 3. To make the PEFC and DMFC micropowerplants comparable, identical inlet molar flow rates of liquid methanol are chosen for both systems, i.e. $n_{CH_3OH,1} = 10$ μmol s^{-1}. The molar ratio of water and methanol at the steam reformer inlet $\varphi_{ref} = 1.1$ and the reformer temperature $T_{ref} = 493$ K. All parameters of the steam reformer are given in Table 1. The steam reformer consists of five reformer tubes to assure satisfactory conversion. The fuel cell is operated at a cell voltage

Table 3
Parameters of the PEFC and DMFC system

Parameters of the PEFC system standard case	Values
Fuel	
Molar methanol flow rate $n_{CH_3OH,1}$ (μmol s^{-1})	10
Vaporizer and pre-heater	
Outer surface areas S_{vap} and S_{pre} (cm^2)	20.0
Heat transfer coefficients α_{vap} and α_{pre} (W m^{-2} K^{-1})	1.0
Steam reformer	
Number of tubes n_{tubes}	5
Molar water/methanol ratio φ_{ref}	1.1
Reformer temperature T_{ref} (K)	493
Outer surface area S_{ref} (cm^2)	20.0
Heat transfer coefficient α_{ref} (W m^{-2} K^{-1})	1.0
PROX reformer	
PROX temperature T_{prox} (K)	443
CO conversion η_{prox}	0.99
Hydrogen PEFC	
Cell length L (m)	0.10
Cell width b (m)	0.05
Fuel cell temperature T_{pefc} (K)	353
Air/fuel ratio λ_{pefc}	1.0
Cell voltage E (V)	0.8
Post-combustor and heat-exchanger	
Outer surface areas S_{pc} and S_{HX1} (cm^2)	5.0
Outer surface area S_{HX2} (cm^2)	2.0
Heat transfer coefficients α_{pc}, α_{HX1}, α_{HX2} (W m^{-2} K^{-1})	1.0
All components	
Total pressure p (MPa)	0.1
Temperature of environment T_0 (K)	298
Temperatures T_1, T_4, and T_9 (K)	298
Temperatures T_2 and T_3 (K)	493
Temperatures T_5, T_6, T_7, and T_8 (K)	353
Temperatures T_{10} (K)	1214
Temperatures T_{11} (K)	798
Temperatures T_{12} (K)	732

Parameters of the DMFC system standard case	
Fuel	
Molar flow rate of methanol $n_{CH_3OH,1}$ (μmol s^{-1})	10
Pre-heater	
Outer surface area S_{pre} (cm^2)	10.0
Heat transfer coefficient α_{pre} (W m^{-2} K^{-1})	1.0
DMFC	
Cell length L (m)	0.10
Cell width b (m)	0.05
Methanol molar concentration $c_{CH_3OH,3}$ (kmol m^{-3})	1.0
Fuel cell temperature T_{dmfc} (K)	353
Air/fuel ratio λ_{dmfc}	1.0
Cell voltage E (V)	0.4
All components	
Total pressure p (MPa)	0.1
Temperature of environment T_0 (K)	298
Temperatures T_1 and T_4 (K)	298
Temperatures T_2, T_3, T_5, T_6, T_7, T_8, T_9, and T_{10} (K)	353
Temperatures T_{11} (K)	400

$E = 0.8$ V, temperature $T_{\text{pefc}} = 353$ K, and air/fuel ratio $\lambda_{\text{pefc}} = 1.0$. For this operational point, satisfactory efficiency is expected. The geometric dimensions of the fuel cell are defined as cell length $L = 10$ cm and cell width $b = 5$ cm. All operating parameters of the standard case are presented in Table 3. The surface areas and the heat transfer coefficients of system components are estimated according to experimental experience. All operating parameters are chosen to guarantee satisfactory power and efficiency. The geometrical parameters and electrochemical properties of the electrodes and membrane are presented in Table 2. In the standard case, the vaporizer, steam reformer, and pre-heater need a total heat input of $Q_{\text{vap}} + Q_{\text{ref}} + Q_{\text{pre}} = 1.87$ W, mainly used by the vaporizer and the steam reformer. This amount can be easily provided by the post-combustor and the heat exchangers ($Q_{\text{pc}} + Q_{\text{HX1}} + Q_{\text{HX2}} = 2.58$ W). Because of the relatively low reformer temperature $T_{\text{ref}} = 493$ K, the conversion efficiency of the steam reformer η_{ref} is less than 45%, which leads to sufficient fuel in the post-combustor for heat generation. The unused part of this heat, $Q_{\text{pc,HX,loss}} = 0.71$ W, is released to the environment. The temperatures of the post-combustor and heat exchangers are significantly higher than those of the vaporizer, steam reformer, and pre-heater. Satisfactory heat transfer is therefore guaranteed. The vaporizer, steam reformer, and pre-heater lose part of their heat input to the environment ($Q_{\text{vap,loss}} + Q_{\text{ref,loss}} + Q_{\text{pre,loss}} = 0.64$ W). The PROX reformer releases less heat to the environment ($Q_{\text{prox}} = 0.19$ W), whereas the fuel cell itself causes relatively high heat loss ($Q_{\text{pefc}} = 1.22$ W). The total heat released to the environment Q_{rel} amounts to 2.76 W.

The exergy destruction by the vaporizer, steam reformer, PROX reformer, and pre-heater is almost negligible in the standard case. Important is the exergy destruction by irreversibilities caused by the fuel cell and the post-combustor with heat exchangers: $A_{\text{dest,pefc}} = 1.17$ W and $A_{\text{dest,pc,HX}} = 1.57$ W, resulting in a total exergy destruction by irreversibilities $A_{\text{dest,irr}}$ of 2.84 W. Due to the complex heat transfer within the fuel cell micropowerplant, the exergy destruction by heat transfer $A_{\text{dest,heat}} = 1.47$ W is significant. The resulting electric power of the PEFC micropowerplant $P = 2.04$ W and the exergetic efficiency $\mu = 28.3\%$. The conversion efficiency of the steam reformer η_{ref} is 44.3% and the utilization factor of hydrogen in the fuel cell amounts to $U_{\text{H}_2} = 99.9\%$. The mole fraction $X_{\text{CO,5}}$ at the fuel cell inlet reaches 2.9 ppm and $X_{\text{CO,7}} = 8.7$ ppm at the outlet. This is significantly lower than the critical CO mole fraction of 10 ppm.

In the following, parameters are varied to investigate their importance on the exergetic efficiency of the entire PEFC micropowerplant. In Figs. 3(a) and 4(a), parameters of the fuel cell itself are changed. In Fig. 3(a), the exergetic efficiency μ and the utilization factor of hydrogen in the fuel cell U_{H_2} are shown as functions of the cell voltage E. For cell voltages below 0.8 V, the exergetic efficiency increases linearly with the cell voltage. At 0.8 V, the exergetic efficiency of the fuel cell system reaches 28.3% and drops dramatically for increasing cell voltage. The reason for this abrupt change in fuel cell efficiency is highlighted in the second graph, depicting the utilization factor of hydrogen. For $E < 0.8$ V, all hydrogen is converted and the maximum current density is reached, resulting in a linear behavior of the power P. For high cell voltages E, the utilization factor U_{H_2}, the electric power P, and the exergetic efficiency μ drop immediately to zero. High cell voltage E indicates a low voltage loss in the fuel cell. Since the voltage loss is directly related to the current density i, the current density has to be low to allow low voltage loss and therefore high cell voltage E. Consequently, low

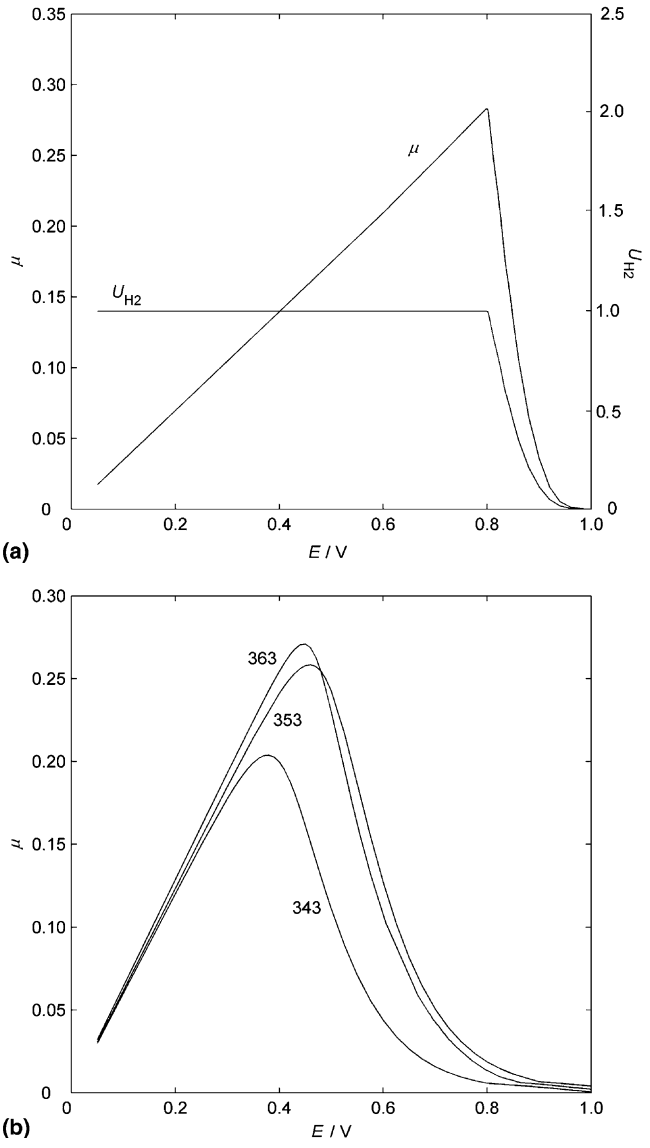

Fig. 3. (a) The exergetic efficiency μ and the utilization factor of hydrogen in the fuel cell U_{H_2} for the PEFC micropowerplant as functions of the cell voltage E. Except for the cell voltage, all parameters are taken from the standard case of the PEFC micropowerplant. (b) The exergetic efficiency μ of the DMFC micropowerplant as a function of the cell voltage E. The labels indicate the fuel cell temperature T_{dmfc} in K. All other parameters are the same as for the standard case of the DMFC micropowerplant.

current density means low hydrogen consumption in the fuel cell. The cell voltage $E = 0.8$ V of the standard case represents optimal conditions with an exergetic efficiency of 28.3%.

In Fig. 4(a), the influence of the fuel cell length L on the exergetic efficiency μ, the utilization factor U_{H_2}, and the mole fraction of CO at the fuel cell outlet $X_{CO,7}$ is shown. For cell lengths below 9.5 cm, only part of the hydrogen input can be converted, which results in a utilization factor $U_{H_2} < 100\%$ and a reduced exergetic efficiency μ. The CO molar flow rate is constant along the anode channel, whereas the total molar flow rate decreases with increasing cell length, because more hydrogen is converted. Therefore, the CO mole fraction is lower for shorter cells. For longer fuel cells, maximum exergetic efficiencies of 28.3% are reached and $X_{CO,7} = 8.7$ ppm, which is still below the critical value of 10 ppm. In this case, all hydrogen can be used.

Some operational parameters of the steam reformer affect the reforming performance and therefore the performance of the fuel cell as well. In Fig. 5, the electric power P, the utilization factor U_{H_2}, the conversion efficiency of the steam reformer η_{ref}, and the mole fraction of CO at the fuel cell outlet $X_{CO,7}$ are presented depending on the temperature of the steam reformer T_{ref} between 450 K and 530 K. The conversion efficiency increases with higher temperatures, since the reforming reaction is faster for high temperatures. On the other hand, the utilization factor of hydrogen in the fuel cell decreases for $\eta_{ref} > 50\%$, because the amount of hydrogen is too high to be used completely by the PEFC of these dimensions and performance characteristics. The increase of reforming conversion and the drop of hydrogen utilization in the fuel cell compensate each other, leading to saturation of electric power P for reformer temperatures above 495 K. Another aspect is the production of CO in the reformer. For higher reformer temperatures, the amount of CO increases. Temperatures above 500 K result in mole fractions of CO at the fuel cell outlet of more than the allowed 10 ppm. Therefore, the steam reformer temperature has to be below 500 K to guarantee that the conversion efficiency of the PROX reformer $\eta_{prox} = 99\%$ is high enough to avoid CO poisoning.

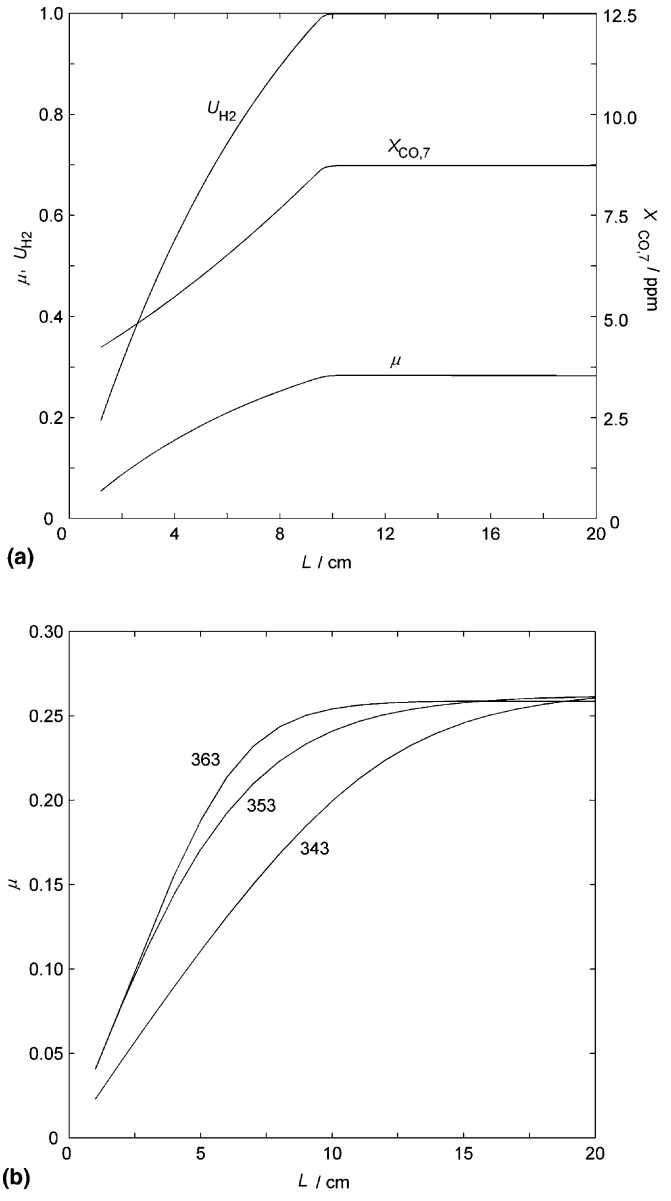

Fig. 4. (a) The exergetic efficiency μ, the utilization factor U_{H_2}, and the mole fraction of CO at the fuel cell outlet $X_{CO,7}$ for the PEFC micropowerplant as functions of the fuel cell length L. Except for the fuel cell length, all parameters are taken from the PEFC standard case. (b) The exergetic efficiency μ of the DMFC micropowerplant as a function of the fuel cell length L. The labels indicate the fuel cell temperature T_{dmfc} in K. Except for the fuel cell length and temperature, all parameters are the same as for the DMFC standard case.

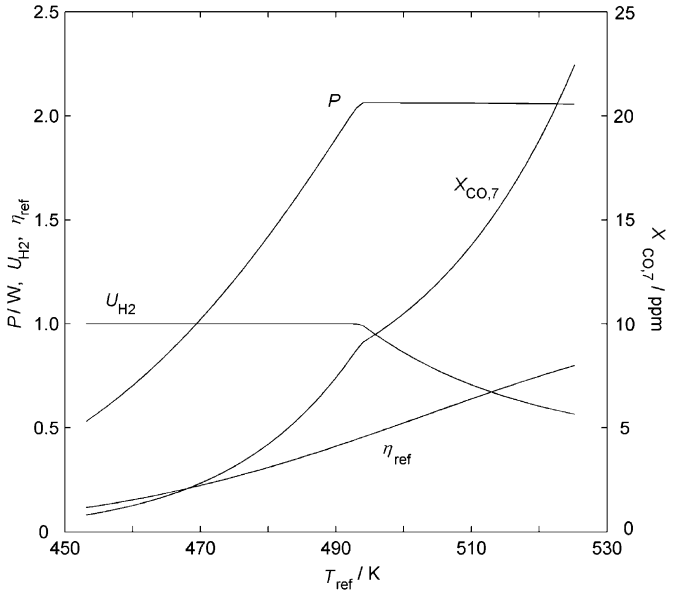

Fig. 5. The electric power P, the utilization factor U_{H_2}, the conversion efficiency of the steam reformer η_{ref}, and the mole fraction of CO at the fuel cell outlet $X_{CO,7}$ for the PEFC micropowerplant as functions of the temperature of the steam reformer T_{ref}. Except for the reformer temperature, the parameters are taken from the PEFC standard case.

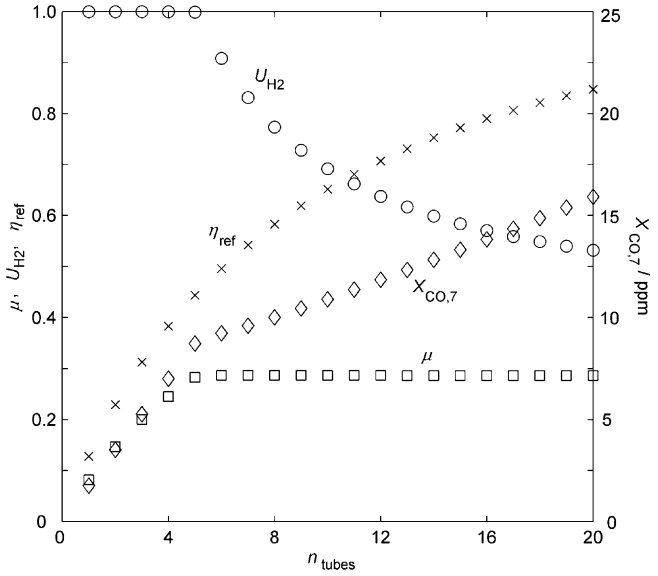

Fig. 6. The exergetic efficiency μ, the utilization factor U_{H_2}, the conversion efficiency of the steam reformer η_{ref}, and the mole fraction of CO at the fuel cell outlet $X_{CO,7}$ for the PEFC micropowerplant as functions of the number of reformer tubes n_{tubes}. Except for n_{tubes}, all parameter are taken from the PEFC standard case.

In Fig. 6, the choice of the number of reformer tubes is investigated. By using more reformer tubes and constant total flow rate of water and methanol, the flow rate per tube is reduced, which results in a higher conversion efficiency η_{ref}, as shown in Section 8.1. Fig. 6 gives the same result: the conversion efficiency of 44.3% for five tubes can be almost doubled by using 20 tubes. The increase of exergetic efficiency μ is limited, since the utilization factor U_{H_2} drops for $n_{tubes} > 5$. For this reason, the exergetic efficiency is constant at 29% for $n_{tubes} > 5$. Another limit is given by the critical CO mole fraction of the fuel cell. For eight tubes, the high performance of the steam reformer already leads to 10 ppm at the fuel cell outlet. The maximum efficiency of 29% can be achieved with six and seven reformer tubes without the risk of CO poisoning.

8.3. DMFC micropowerplant

The electric power and exergetic efficiency of the DMFC micropowerplant are calculated for the standard case defined in Table 3. To render the DMFC system comparable to the PEFC micropowerplant of the previous subsection, both systems have the same molar flow rate of liquid methanol at the inlet, i.e. $n_{CH_3OH,1} = 10\ \mu mol\ s^{-1}$. For the inlet flow of the fuel cell, the molar concentration of methanol is $c_{CH_3OH,3} = 1.0\ kmol\ m^{-3}$, indicating 1 M methanol solution and a water/methanol ratio $\varphi_{dmfc} = 53.35$. The cell voltage $E = 0.4$ V for the standard case, which is lower than typical cell voltages of the PEFC. This is attributed to the higher voltage losses in the DMFC compared to the PEFC. The cell length $L = 10$ cm and the cell width $b = 5$ cm. The DMFC is operated at a temperature $T_{dmfc} = 353$ K and a stoichiometric air/fuel ratio $\lambda_{dmfc} = 1.0$. The exhaust gas of the post-combustor has a temperature $T_{11} = 400$ K. All operating parameters of the standard case are presented in Table 3. The surface area and the heat transfer coefficient of the pre-heater are estimated according to experimental experience. All operating parameters of the DMFC are chosen to guarantee satisfactory electric power and exergetic efficiency. The geometrical parameters and electrochemical properties of the electrodes and membrane are presented in Table 2.

Due to the simpler system setup and the relatively low methanol utilization in the fuel cell, the heating of the entire system is much less crucial than for a PEFC system. Since only methanol has to be pre-heated, the pre-heater needs $Q_{pre} = 0.20$ W, which can be easily provided by the post-combustor releasing $Q_{pc} = 0.37$ W. Because of methanol cross-over and diffusion barriers, only 75.0% of the methanol are converted in the fuel cell and the post-combustor gets enough burnable fuel. The total heat released from the pre-heater $Q_{pre,loss}$, the fuel cell Q_{dmfc}, and the excess heat of the post-combustor $Q_{pc,loss}$ sum up to $Q_{rel} = 5.44$ W, where the fuel cell releases the main part of Q_{rel} with $Q_{dmfc} = 5.24$ W.

The exergy destruction by the pre-heater and the mixer is almost negligible. The exergy destruction by irreversibilities $A_{dest,irr}$ results in 4.80 W, where most of the exergy destruction is caused by the fuel cell ($A_{dest,dmfc} = 4.30$ W) and the post-combustor ($A_{dest,pc} = 0.42$ W). The exergy destruction by heat transfer and the separator is significantly less important ($A_{dest,heat} + A_{dest,sep} = 0.44$ W). The resulting electric power of the DMFC micropowerplant $P = 1.73$ W and the exergetic efficiency $\mu = 24.1\%$ are lower than the comparable standard case of the PEFC with $\mu = 28.3\%$. The methanol cross-over coefficient ω_{CH_3OH}, indicating the molar amount of methanol crossed over compared to the methanol inlet flow, is 18.1%. The remaining methanol from the anode is burnt in the post-combustor.

A parametric study is carried out to investigate the importance and influence of certain operational parameters and to show how the generated electric power and exergetic efficiency can be improved compared to the presented standard case. In Fig. 3(b), the influence of the cell voltage E on the exergetic efficiency μ is shown. For the DMFC, the maximum efficiency μ is reached at lower cell voltages than for the PEFC. Higher temperatures lead to faster reaction and diffusion processes, lower ohmic resistance, higher maximum power, and higher efficiency. For a fuel cell temperature of 343 K (353 K, 363 K), the maximum exergetic efficiency amounts to 20.4% (25.8%, 27.1%). Small changes of the cell voltage have dramatic effects on the efficiency. Therefore, the choice of a reasonable cell voltage is essential for high fuel cell efficiency.

In Fig. 4(b), the exergetic efficiency μ of the entire DMFC micropowerplant is plotted as a function of the cell length L. The exergetic efficiency increases with higher cell length, since the utilization of methanol U_{CH_3OH} increases for longer cells. For cells longer than 20 cm, all methanol

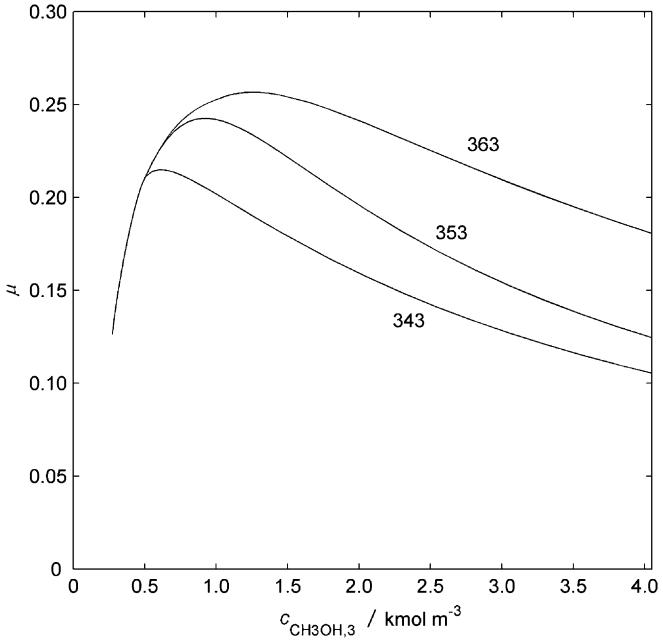

Fig. 7. The exergetic efficiency μ as a function of the molar concentration of methanol at the fuel cell inlet $c_{CH_3OH,3}$. The labels indicate the fuel cell temperature T_{dmfc} in K. Except for $c_{CH_3OH,3}$ and the fuel cell temperature, all parameters are the same as for the standard case of the DMFC system.

can be converted by the fuel cell and a maximum exergetic efficiency of 26.0% is reached. The exergetic efficiency for a cell length $L = 10$ cm and $T_{dmfc} = 353$ K is already close to the maximum exergetic efficiency. Therefore, the choice of $L = 10$ cm in the standard case is reasonable.

Considering the effect of methanol cross-over and mass transfer limitations, the molar concentration of methanol at the fuel cell inlet $c_{CH_3OH,3}$ is crucial for the DMFC. High methanol concentrations lead to voltage losses due to cross-over, whereas low concentrations decrease the limiting anode current density i^a_{lim}, as shown in Fig. 7. The exergetic efficiency μ attains maxima between 0.5 kmol m^{-3} and 1.5 kmol m^{-3}, which agrees very well with results from the literature [12,14]. For higher fuel cell temperatures T_{dmfc}, the maximum achievable efficiency and optimal methanol concentration are higher. The maximum exergetic efficiency μ for $T_{dmfc} = 343$ K is achieved at a molar concentration $c_{CH_3OH,3} = 0.55$ kmol m^{-3} or 0.55 M and amounts to 21.6%. For 353 K and 0.95 M, the maximum efficiency is 24.2%, and $\mu = 25.7\%$ is reached for 363 K and 1.2 M, respectively.

9. Conclusions

The numerical models developed in this study simulate the characteristic behavior of a methanol packed bed steam reformer, a PEFC, and a DMFC under different operating conditions. The electrochemical processes and the species diffusion phenomena in the fuel cells are modeled as functions of the thermodynamic state. The influence of operational and geometric parameters on the efficiency of PEFC and DMFC micropowerplants are investigated according to the first and the second law of thermodynamics. The efficiency of both micropowerplants may be increased significantly by performing at certain operating conditions. Useful information about optimal conditions can be deduced from the models presented in this study.

The results show that the PEFC micropowerplant achieves higher exergetic efficiency than the DMFC micropowerplant for the same inlet flow rate of methanol. By optimizing the operational conditions, the presented PEFC micropowerplant generates about 2.2 W at an exergetic efficiency of approximately 30%. The comparable DMFC micropowerplant achieves at optimized conditions 1.8 W and 25% exergetic efficiency. However, this difference in efficiency is partly compensated by the fact that the DMFC system is significantly simpler and smaller because of the absence of fuel reforming and the less complex heat transfer within the system. In the PEFC micropowerplant, three components at different temperature levels have to be heated, whereas the DMFC system only needs heating of one component. The heat management in the entire system is therefore significantly simpler. The simpler DMFC setup might be more attractive for small and portable approaches than the more efficient but larger PEFC system. The developed fuel cell models can be modified and extended to consider different types of fuel or different system configurations. Further improvement could be achieved by extending the simplified flow model in the fuel cell channels and by using a more complex heat transfer model.

References

[1] M.A. Rosen, Comparison based on energy and exergy analyses of the potential cogeneration efficiencies for fuel-cells and other electricity-generation devices, Int. J. Hydrogen Energy 15 (4) (1990) 267–274.
[2] J.C. Amphlett, K.A.M. Creber, J.M. Davis, R.F. Mann, B.A. Peppley, D.M. Stokes, Hydrogen-production by steam reforming of methanol for polymer electrolyte fuel-cells, Int. J. Hydrogen Energy 19 (2) (1994) 131–137.
[3] H.G. Park, M.-T. Lee, F.K. Hsu, C.P. Grigoropoulos, R. Greif, C.-H. Lin, Transport in a methanol steam reformer as the fuel processor for fuel cell systems, IMECE2004-61208, in: Proceedings of IMECE2004.
[4] V. Gurau, F. Barbir, H. Liu, An analytical solution of a half-cell model for PEM fuel cells, J. Electrochem. Soc. 147 (7) (2000) 2468–2477.
[5] S.H. Chan, S.K. Goh, S.P. Jiang, A mathematical model of polymer electrolyte fuel cell with anode CO kinetics, Electrochim. Acta 48 (2003) 1905–1919.
[6] T.E. Springer, T. Rockward, T.A. Zawodzinski, S. Gottesfeld, Model for polymer electrolyte fuel cell operation on reformate feed, J. Electrochem. Soc. 148 (1) (2001) A11–A23.
[7] T.E. Springer, T.A. Zawodzinski, S. Gottesfeld, Polymer electrolyte fuel-cell model, J. Electrochem. Soc. 138 (8) (1991) 2334–2342.
[8] S.H. Chan, C.F. Low, O.L. Ding, Energy and exergy analysis of simple solid-oxide fuel-cell power systems, J. Power Sour. 103 (2) (2002) 188–200.
[9] M.W. Chase, NIST-JANAF Thermochemical Tables, fourth ed., J. Phys. Chem. Ref. Data, Monograph 9 (1998) 1–1951.
[10] M.J. Moran, H.N. Shapiro, Fundamentals of Engineering Thermodynamics, fourth ed., Wiley, New York, 1999, p. 848.

[11] M.J. Castaldi, R.S. Boorse, S. Roychoudhury, P.V. Menacherry, W.C. Pfefferle, A compact, lightweight, fast-response preferential oxidation reactor for PEM automotive fuel cell applications, Precision Combustion, Inc., 410 Sackett Point Road, North Haven, CT 06473.

[12] A.A. Kulikovsky, A method for analysis of DMFC performance curves, Electrochem. Commun. 5 (12) (2003) 1030–1036.

[13] R.B. Bird, W.E. Stewart, E.N. Lightfoot, Transport Phenomena, Wiley, New York, 1960, p. 505.

[14] H. Dohle, K. Wippermann, Experimental evaluation and semi-empirical modeling of U/I characteristics and methanol permeation of a direct methanol fuel cell, J. Power Sour. 135 (1–2) (2004) 152–164.